

Microfocusing of Hard X-rays with Cylindrically Bent Crystal Monochromators

C. Schulze,^{a*} U. Lienert,^{b,c} M. Hanfland,^b M. Lorenzen^b and F. Zontone^b

^aSwiss Light Source, PSI, CH-5232 Villigen PSI, Switzerland, ^bEuropean Synchrotron Radiation Facility, BP 220, F-38043 Grenoble CEDEX, France, and ^cRisø National Laboratory, Materials Department, DK-4000 Roskilde, Denmark. E-mail: schulze@psi.ch

(Received 4 August 1997; accepted 24 October 1997)

High-energy X-ray focusing with bent-crystal monochromators is known to be hampered by so-called depth or crystal-thickness aberrations. A theoretical model of focus broadening based on the geometrical theory of X-ray diffraction in slightly deformed crystals is presented and compared with experimental data. First, it is shown that depth broadening can be avoided in the Laue geometry by an appropriate choice of asymmetry angle. Based on this finding, a monochromator for high-pressure diffraction experiments has been designed and a source-size-limited focal spot below 10 μm is observed. As a consequence of the box-shaped rocking curve of bent Laue crystals, the focus is free of long-ranging tails. Diffraction patterns of standard powder samples were recorded on imaging plates and a theoretical description of the energy-dispersion-related peak broadening is given. Finally, diffraction patterns of N_2 at 180 kbar demonstrate the excellent data quality achievable with this monochromator.

Keywords: bent-crystal monochromators; microfocusing; geometrical theory; polychromatic focus broadening.

1. Introduction

Bent-crystal monochromators have been in use at synchrotron radiation facilities for more than two decades to monochromatize and focus the X-ray beam (Barrington Leigh & Rosenbaum, 1974). They offer several advantages over mirrors and multilayers in hard X-ray microfocusing. Spherical aberrations are smaller due to the larger angle of incidence, and surface roughness and slope errors have no deteriorating effect because the beam is reflected by the intrinsically perfect lattice planes.

However, with the advent of third-generation synchrotron sources it became evident that the achievable focus size was in general larger than the demagnified image of the source. Part of the effect was attributed to the polychromatic aberration (Takeshita, 1995).

We present a model of focus broadening based on the geometrical theory of diffraction that takes into account the trajectory of the beam in the distorted crystal as well as the boundary conditions at the exit surface. Experimental results obtained in Bragg and Laue geometry corroborate the theory.

High-pressure diffraction experiments require focus dimensions of 25 μm at about 30 keV photon energy, where the high energy is essential to reduce the absorption by the diamond in the anvil cell. In order to minimize the background intensity from the gasket, the focal spot should be free of a long tail and good positional (thermal)

stability is essential. Cylindrically bent Laue crystal monochromators provide all these properties.

2. Bent-crystal focusing

2.1. Geometrical focusing

Focusing of X-rays by bent crystals is based on a change in the Bragg plane orientation. In meridional focusing the relation between the source distance, p , and the focal distance, q , is given by

$$q = q_0 / (2 - p_0/p), \quad (1)$$

where

$$p_0 = R\gamma_0 = R \cos(\chi \pm \theta_B),$$

and

$$q_0 = R|\gamma_h| = R|\cos(\chi \mp \theta_B)|$$

are for monochromatic focusing. The asymmetry angle, χ , is given by the angle between the crystal surface normal and the Bragg planes, and the lower signs correspond to a beam incident between these two directions. The bending radius, R , is positive when the beam is incident on the concave side, and p is positive for a real source.

2.2. Bent-crystal rocking curves

The geometrical focusing as described by (1) is realised only for an infinitesimally narrow rocking curve. Bent-

crystal rocking curves are broadened with respect to the intrinsic Darwin width, and the deviation of the focus size from geometrical optics can be significant. The broadening is due to changing reciprocal lattice vector orientations as well as d -spacing and asymmetry-angle variations. For cylindrically bent Laue crystals the rocking-curve broadening, $\Delta\theta$, is given by

$$\Delta\theta = \pm (T \tan \chi / R \cos^2 \theta_B) (\gamma_h / \gamma_0)^{1/2} \times \{1 + (\cos 2\chi + \cos 2\theta_B) / 2 \times [1 - (s_{13} + s_{15} \cot \chi) / s_{11}]\}, \quad (2)$$

where T denotes the crystal thickness and s_{ij} are the elastic compliances for the given crystal orientation and asymmetry angle (Schulze & Chapman, 1995). The rocking-curve broadening can lead to a substantial gain in integrated reflectivity as compared with the flat-crystal case, with the upper limit set by the kinematical reflectivity.

The models describing the diffraction of X-rays in distorted crystals can be separated into two classes which differ in the amount of the admitted variation of the amplitudes of the electric field on transition through the crystal. The geometrical theory as outlined by Penning & Polder (1961) and Kato (1963, 1964) does not cover the creation of new wavefields for strong crystal deformation, which is accounted for by the wave-optical theory developed by Takagi (1969). However, Gronkowski & Malgrange (1984) demonstrated that the theories are equivalent in terms of the propagation of the X-ray beam in the bent crystal, and Krisch (1993) showed the same for the rocking curves. The only exception is the range of quasi-total reflectivity in the Bragg case, where the strong complex component of the wavefields conflicts with the properties of well behaved beams, which form the foundation of the geometrical theory. Yet, in the hard X-ray range, the intrinsic Darwin width is usually negligible compared with the rocking-curve broadening, $\Delta\theta$, and the contribution of the total-reflection range can be safely neglected in the derivation of the focusing properties of bent Bragg crystals.

2.3. Polychromatic focusing

When a polychromatic pencil beam enters the bent crystal, rays of different energies within the rocking curve will propagate on different trajectories inside the Borrmann fan. The trajectories are of hyperbolic shape and the different energies are spread over the Borrmann fan at the exit surface. In order to determine the reflection angle for different rays, we have to take two boundary conditions into account. First, the tangential components of the wavevectors have to be constant at the crystal surface, which also holds for the flat-crystal case (Matsushita & Kaminaga, 1980). Second, due to the crystal curvature, the reciprocal lattice vectors change orientation over the Borrmann fan. Apart from the flanks of the rocking curve the two terms depend linearly on energy and sum to the

total divergence of the reflected beam:

$$\Delta\theta_{\text{poly}} = (1 + b)\Delta\theta_0 + \text{BF}/R, \quad (3)$$

where $b = \cos(\chi \pm \theta) / \cos(\chi \mp \theta)$ denotes the asymmetry factor, $\Delta\theta_0$ is the rocking-curve width and BF is the size of the Borrmann fan. The second term in (3) represents the rotation of the reciprocal lattice vector and is not present in the flat-crystal case. The distinct position-angle coupling over the Borrmann fan gives rise to a real or virtual polychromatic focus, with the polychromatic focus length given by

$$q_{\text{poly}} = \text{BF}\gamma_h / \Delta\theta_{\text{poly}}. \quad (4)$$

In general, the polychromatic and geometric foci do not coincide, giving rise to the focus broadening known as ‘crystal depth broadening’. However, it can be seen from (2) and (3) that, for an adequate choice of the crystal asymmetry angle, the two focal lengths become identical. In this case the resulting focus size is limited by the

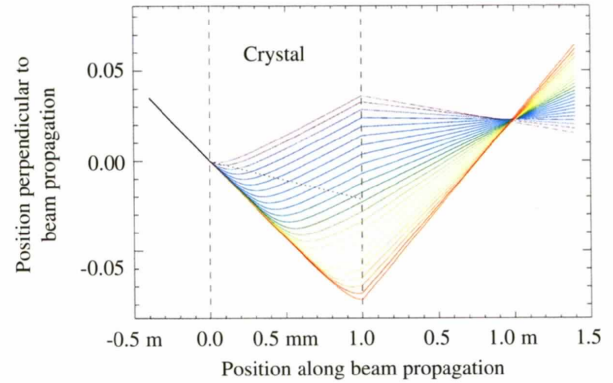


Figure 1

Trajectories of a polychromatic pencil beam inside and outside of the bent Laue crystal monochromator. The dotted line indicates the Bragg planes. The colours represent the energies within the 50% reflectivity limit of the rocking curve. The dimensions inside the crystal are given in millimetres, those outside of it in metres. Note that $\Delta\theta$ changes sign when the beam is incident on the lower (convex) side of the Bragg planes, giving rise to an almost parallel diffracted beam. In this case, geometrical and polychromatic foci are far apart and the focus has the size of the Borrmann fan. The geometrical focal length is 1 m.

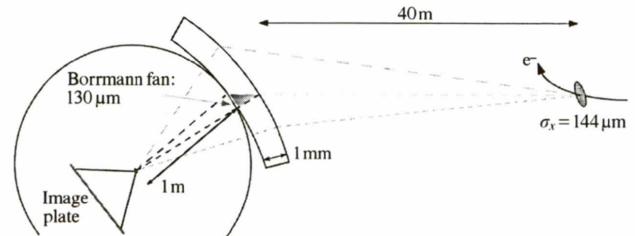


Figure 2

Experimental set-up in high-pressure diffraction experiments. The outer thin lines correspond to the geometrical focus, while the inner bold lines represent the polychromatic focus. The length of the dashes symbolizes the wavelength. Energy 30 keV, Si(111) reflection, asymmetry angle 1.28° , bending radius -2.05 m.

demagnification of the source size only. This situation is depicted in Fig. 1.

Different limitations exist for the Laue and the Bragg cases. In the latter it is only in the symmetric case ($b = -1$, 1:1 focusing) where the first term in (3) vanishes and the second matches the geometrical beam divergence independently of the energy. In the focusing Laue geometry the condition can be fulfilled for all magnifications for slightly asymmetric crystals. However, since the Borrmann fan width varies as a function of energy, while the geometrical focal length remains almost constant, a given asymmetry angle corresponds to one energy only and deviations cause a focus broadening.

3. Experimental set-up

A focusing Laue monochromator was designed for high-pressure diffraction experiments to deliver a focal spot diameter of $25\ \mu\text{m}$ at 30 keV photon energy. The corresponding experimental set-up at ESRF ID9 (Mason, 1995) and the crystal parameters are shown in Fig. 2. The large focal distance of 1 m provides sufficient space for bulky pressure cells and auxiliary equipment. The (111) reflection of silicon was chosen because it has the smallest Borrmann fan. In consequence, the depth of field is the largest and the focus size displays the lowest sensitivity to energy changes. For the crystal parameters, as summarized in Fig. 2, the integrated reflectivity of the bent Laue monochromator ($29.2\ \mu\text{rad}$) exceeds those of the flat Bragg or Laue counterparts by factors of 2.5 and 6, respectively.

4. Experimental results

The focusing properties of the bent-crystal monochromators were tested at the ESRF optics beamline BM5 (Mason, 1995). The source distance, p , was 40 m.

4.1. Focusing

Fig. 3 depicts the profile of the horizontally focused beam as obtained from the derivative of a knife-edge scan. The incident beam size was $1.5 \times 0.1\ \text{mm}^2$ ($H \times V$). The focus is more than 15 times smaller than the Borrmann fan. It exceeds the size of the demagnified source ($6.5\ \mu\text{m}$) since the energy was 27.15 instead of 30 keV. Because of the box-shaped rocking curve, the focus profile is free of long-ranging tails and the only background arises from Compton and thermal diffuse scattering. Moreover, owing to the almost normal beam incidence, slightly asymmetric Laue crystal foci display little spherical aberration. Fig. 4 represents the focus broadening resulting from spherical aberrations for different horizontal slit sizes for a bending radius of $-2.05\ \text{m}$. Even for a slit size as large as 5 mm, an almost Gaussian beam profile can be achieved by moving the sample slightly out of focus.

4.2. Diffracted beam divergence

It was stated in the previous section that the formula for calculating the divergence of the diffracted beam is also valid in the Bragg case. Fig. 5 represents a comparison of experimental and theoretical values as calculated using (3). The agreement is satisfactory. It should be noted that the Bragg geometry is less suited for microfocusing. For demagnifying asymmetric cuts ($b < -1$), polychromatic divergence and reciprocal-lattice-vector rotation are of opposite sign, *i.e.* $\Delta\theta_{\text{poly}}$ is small and consequently the polychromatic focal length exceeds the geometrical one significantly. For asymmetry factors b between -1 and 0 , the mismatch of the two focal lengths is reduced, but in this case the shallow beam incidence causes severe spherical aberrations.

4.3. Energy dispersion

The strong crystal curvature in the focusing Laue geometry results in a substantial variation of the angle of incidence across the crystal surface giving rise to a broad energy band and a large divergence of the focused beam, both effects deteriorating the resolution of powder dif-

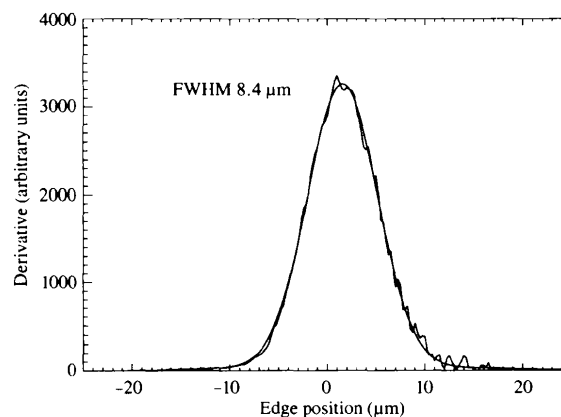


Figure 3

Focus profile obtained from the derivative of a knife-edge scan and a Gaussian fit to the data. Demagnification 52:1, bending radius $-1.57\ \text{m}$.

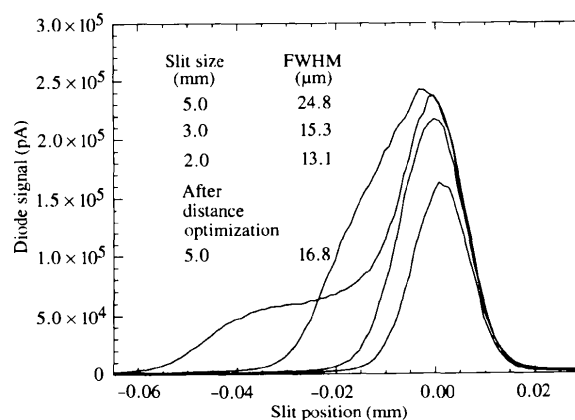


Figure 4

Spherical aberrations as a function of the horizontal acceptance.

fraction patterns. The total angular width of a powder ring in the scattering plane at Bragg angle θ_3 due to the energy band ΔE and convergence angle $\Delta\Psi$ of the focused beam is given by

$$\Delta\Psi_{\text{tot}} = \Delta\Psi \pm 2\Delta E/E \tan \theta_3, \quad (5)$$

where the negative sign corresponds to the non-dispersive side. When sample and monochromator lattice spacings are equal, the resulting divergence of the diffracted beam on the non-dispersive side is equal to that of the primary beam. Fig. 6 shows a comparison of the experimental and theoretical angular widths of the diffraction rings of a standard silicon powder sample.

4.4. High-pressure diffraction

A water-cooled version of the Laue monochromator was installed at ID9. Vertical focusing is achieved by means of

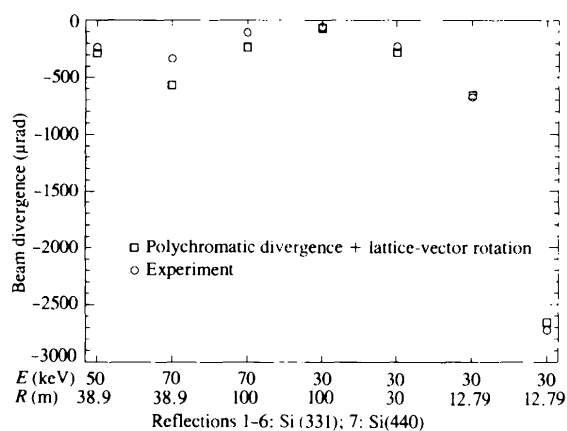


Figure 5

Comparison of theoretical and experimental divergence of the diffracted beam for different reflections, energies and asymmetry factors in Bragg geometry. The deviations for 70 keV are probably due to a small error of the asymmetry angle, causing a significant change in b .

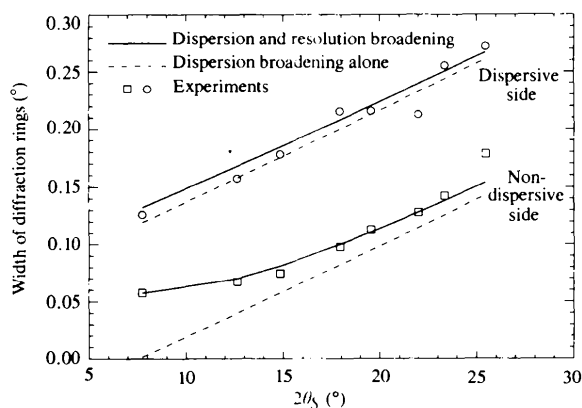


Figure 6

Width of powder diffraction peak from Si recorded on an imaging plate. The divergence of the primary beam was 25 μrad , corresponding to an energy band width of 0.76%, and the sample-plate distance was 334 mm. The dashed lines represent the theoretical width without the contribution of the image-plate resolution.

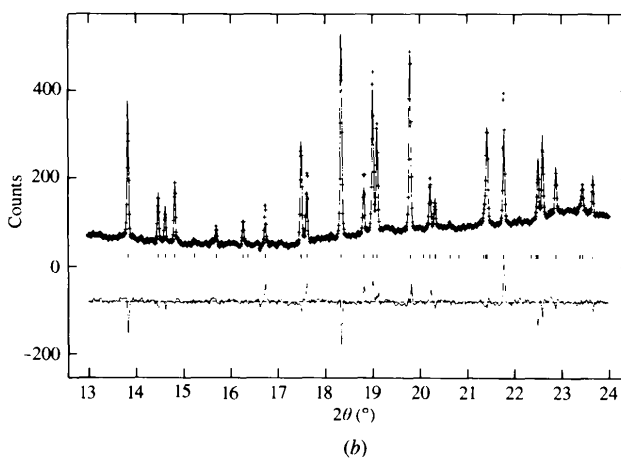
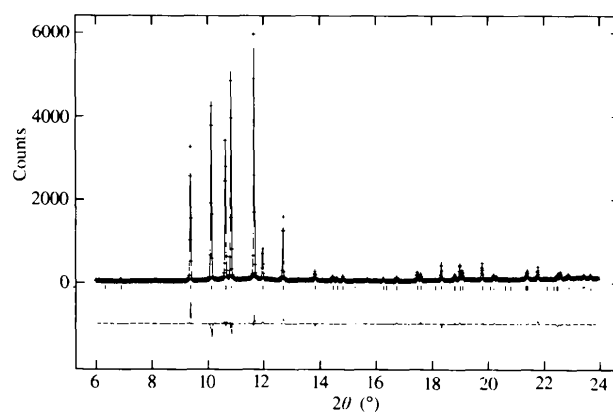
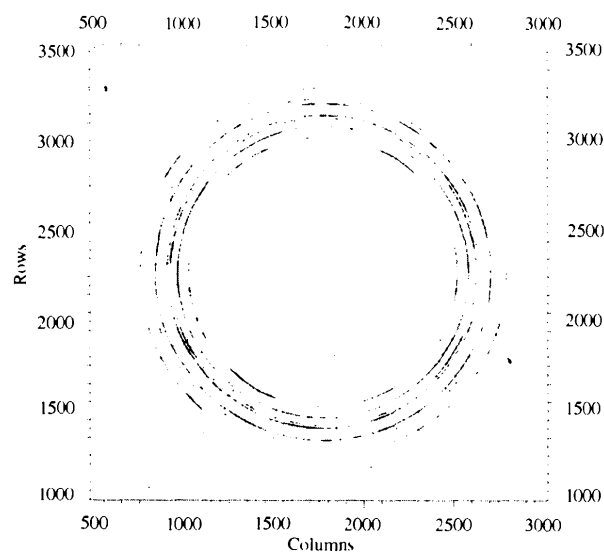


Figure 7

(a) Diffraction image of N_2 at 180 kbar. In order to reduce the background from inelastic scattering from the diamonds, a diffraction image of the empty cell was subtracted. The sample had a diameter of 100 μm and a thickness of 20 μm . (b) Measured (crosses) and calculated (line) diffraction patterns.

a cylindrically bent platinum-coated mirror. The focal spot dimensions are smaller than $15 \times 30 \mu\text{m}^2$. The flux, as measured by means of a silicon diode, is 7.6×10^{10} photons s^{-1} at 204 mA ring current and an energy band path of 10^{-3} , equivalent to 1.3×10^8 photons s^{-1} (100 mA) $^{-1}$ μm^{-2} . Typical image-plate exposure times are 5 min at 150 mA. Because of the low absorbed power in the thin Laue monochromator, the thermal stability is excellent after a warm-up period of 10 min.

The monochromator is now routinely used for high-pressure experiments at ID9. The high flux in conjunction with the clean beam profile allows data of unprecedented resolution and sensitivity to be collected. Fig. 7 shows an example of a powder diffraction image of N_2 at 180 kbar. The weak reflections beyond 13 $^\circ$ were observed for the first time, with the upper limit of 2 θ being set by the anvil-cell opening angle (Hanfland *et al.*, 1998).

5. Conclusions and outlook

The so-called 'depth broadening' of bent-crystal monochromators can be overcome by a correct choice of the crystal asymmetry angle, allowing source-size-limited foci to be achieved. Recently, a focus size of $1.2 \mu\text{m}$ at 90 keV photon energy was measured using a bent Laue crystal monochromator (Lienert *et al.*, 1998) and, theoretically, diffraction-limited foci of the order of $0.2 \mu\text{m}$ should be achievable.

The polychromatic focusing geometry is optimally suited for energy-dispersive experiments, such as dispersive-EXAFS, as well as techniques which tolerate a larger energy band path, such as SAXS. In other applications the detrimental effect of the large energy bandwidth can be overcome when dispersion compensation can be applied.

References

- Barrington Leigh, J. & Rosenbaum, G. (1974). *J. Appl. Cryst.* **7**, 117–121.
- Gronkowski, J. & Malgrange, C. (1984). *Acta Cryst.* **A40**, 515–522.
- Hanfland, M., Lorenzen, M., Wassilew-Reul, C. & Zontone, F. (1998). *The Review of High Pressure Science and Technology*. In the press.
- Kato, N. (1963). *J. Phys. Soc. Jpn.*, **18**, 1785.
- Kato, N. (1964). *J. Phys. Soc. Jpn.*, **19**, 67–77; 971–985.
- Krisch, M. H. (1993). Thesis, University of Dortmund, Germany.
- Lienert, U., Schulze, C., Honkimäki, V., Tschentscher, T., Garbe, S., Hignette, O., Horsewell, A., Lingham, M., Poulsen, H. F., Thomson, N. B. & Ziegler, E. (1998). *J. Synchrotron Rad.* **5**. In the press.
- Mason, R. (1995). Editor. *ESRF Beamline Handbook*. ESRF, Grenoble, France.
- Matsushita, T. & Kaminaga, U. (1980). *J. Appl. Cryst.* **13**, 472–478.
- Penning, P. & Polder, D. (1961). *Philips Res. Rep.* **16**, 419–440.
- Schulze, C. & Chapman, D. (1995). *Rev. Sci. Instrum.* **66**(2), 2220–2223.
- Takagi, S. (1969). *J. Phys. Soc. Jpn.*, **26**, 1239–1253.
- Takeshita, K. (1995). *Rev. Sci. Instrum.* **66**(2), 2238–2240.